Challenging Glass 6 - Conference on Architectural and Structural Applications of Glass
Louter, Bos, Belis, Veer, Nijsse (Eds.), Delft University of Technology, May 2018.
Copyright © with the authors. All rights reserved.
ISBN 978-94-6366-044-0, https://doi.org/10.7480/cgc.6.2160

Dimensioning of Elastic Adhesive Joints with Complex Geometries? – A Systematic Approach beyond ETAG 002

Thomas Scherer, Wolfgang Wittwer, Christian Scherer, Ernst Semar
Kömmerling Chemische Fabrik GmbH, Pirmasens, Germany,
contact e-mail: christian.scherer@koe-chemie.de

The current European standard for dimensioning silicone adhesive joints in structural glazing applications is defined in the ETAG 002. Although there are several decades of field experience with this standard it still has some major limitations and mainly uses an empirical concept based on an average force by area tension engineering approach. In addition there are a number of other restrictions for example the limitation of specific substrates and rectangular shaped joints with defined aspect ratios as well as the exclusion of joints with non-coplanar surfaces. The presented investigations are based on a combined numerical and experimental concept and demonstrate that appropriately designed elastic adhesive joints with complex geometries excluded by common standards can be evaluated and validated in a systematic and reliable way. The experimental test may easily be combined with well-established and proven aging test schemes, for which long-term reliable field experience is available. In addition any desired safety factor can be added.

Keywords: ETAG 002**,** glass joint dimensioning, silicone, hyperelastic adhesive

1. Introduction

The desire for completely flat glass surfaces without visible fixings triggered a worldwide trend towards glued all-glass facades in the 1980's and this continues today. In these Structural Glazing (SG) or Structural Sealant Glazing (SSG) facade is defined where the support structure is not visible from the outside. Therefore, these frames are nowadays an integral part of contemporary architecture and create a stunning architectural look to the building. The SG optics embodies both transparency and lightness in the facade design. Over the past decades silicone sealants have been successfully used in structural glazing applications to bond architectural glass to curtain wall framing in high performance building facades (for example see Fig. 1).

Fig. 1 Glass Sphere and pavilions of the EXPO 2017 in Astana Kasachstan

The basic design theory on how to correctly size the structural silicone joint is defined in the ETAG 002 which was published between September 1998 and May 2002 by the European Organization for Technical Approvals (EOTA) (EOTA - European Organisation for Technical Approvals 2012). The guideline mainly uses an empirical approach for the joint dimensioning. During the early days of structural glazing, silicone sealants had only a limited performance

history in an accelerated testing regime, using artificial aging methods to demonstrate the long-term integrity and safety of the silicone bonding,. However, the scope of the ETAG 002 lists some major restrictions for examplet structural sealant has to be based on silicones therefore the joints are restricted to linear beads with a rectangular shape and an adhesion of the silicone on three surfaces is not permissible (Klosowski and Wolf 2016). Modern glass facades demand not only slimmer profile views and therefore smaller silicone joints but also often require more complex designs– leading e.g. to a U-type (Hagl 2008) or L-shaped bonding geometry. These advanced bonding designs are beyond the scope of the ETAG 002 and lead to significantly different mechanical characteristics. This study demonstrates how a combined numerical and experimental concept can be used for the design and dimensioning of complex joint geometries.

From a physical point of view, silicones are grouped as elastomers and therefore show typical behaviour in line with hyperelastic material thus separating them significantly from the classical linear behaviour of structural engineering materials such as aluminium, steel or glass. Due to their almost perfect incompressibility and high elastic strain levels silicones show hyperelastic stress-strain behaviour. In addition silicones - especially filled ones - show typical rubber-like features such as the Mullins effect (Mullins 1948) i.e. softening after loading and visco-elasticity which leads to additional difficulties in developing a suitable material law. The utilized finite element analysis (FEA) calculations are based on a hyperelastic material law for the high temperature resistant two component silicone structural adhesive HelioBond PVA 200 D. The parameters used have been identified by a least square minimization of well-matched uniaxial tensions, uniaxial compression and simple shear tests and furthermore validated by butt-joint-tests. They provide the opportunity to calculate overall deformations and local strains for complex geometries under different specified load cases (wind, snow, thermal elongation, etc.). In this study a material law is used to dimension an L-shaped silicone adhesive joint that bonds the cover glass of a solar thermal collector to its aluminium or GFRP (Glass Fibre Reinforced Polymer) frame. Modelling a set of different load cases by numerical simulation shows that the calculated values for the local strain energy densities reach their maximum in the corners of the solar thermal collector. To prove the long term durability of the joint, fatigue tests were carried out on 100 mm x 100 mm sized section cut from the corner of the collectors. The amplitudes for the experimental proof were taken from calculations of combined load cases and then exaggerated by a safety factor of 2 for in-plane and out-of-plane deformations. The corner sections cut test specimens are exposed to this resulting deformation level and subsequently do not show visible or measureable damage after $2 \cdot 10^6$ load cycles. The numerical calculations and component tests in this work package demonstrate an approach that makes it possible to dimension an adhesive joint with more complex geometry than that allowed in ETAG 002.

2. Numerical Calculation

2.1. Material Model for the Adhesive Joint

The goal of this work is the dimensioning and proving of the mechanical strength of an adhesive joint used in a solar thermal energy collector in accordance its ULS (ultimate limit state), where common joint geometries are far beyond the given restrictions of ETAG 002. Since the glass pane and the frame will not become critical in the conditions relevant to these extended geometries they are not in the focus of this investigation. Therefore they can be represented with standard linear elastic material models. However the adhesive shows a nonlinear material behaviour even for relatively small strains. The material behaviour of the investigated adhesive depends to some extent on

- Temperature
- Strain Rate

and more importantly

- Mode of Load (tension, shear, compression, …)
- Load History

This means a suitable material model has to either cover the effects or alternatively the model parameters must be consistent with the conditions present in the field (e.g. temperature, strain rate, etc…). In this work a hyperelastic material model was chosen to represent the properties of the silicone sealant used i.e Kömmerling HelioBond PVA 200 D. Numerical models for hyperplastic material behaviour are based on the formulation of a strain energy density function dependant on strain invariants or principal stretches. The definition of the strain invariants is given in the following equations:

$$I_1 = {\lambda_1}^2 + {\lambda_2}^2 + {\lambda_3}^2 \qquad (1)$$

$$I_2 = \lambda_1\lambda_2 + \lambda_1\lambda_3 + \lambda_2\lambda_3 \qquad (2)$$

$$I_3 = {\lambda_1}^2 \cdot {\lambda_2}^2 \cdot {\lambda_3}^2 \qquad (3)$$

Where I_3 are the strain invariants and λ_1 are the principal stretches. There are numerous formulations of strain energy density functions to define a hyperelastic material behaviour these are are available in commercial Finite-Elements software (such as the Ogden (Ogden 1972, Dassault Systemes Simulia Corp. 2016) or Arruda-Boyce (Arruda and Boyce 1993, Dassault Systemes Simulia Corp. 2016) formulations). In order to find the one that matches best with the measured material behaviour the material parameters for the most common formulations have been identified, and the one that represents the experimentally measured behaviour most closely, is chosen.

Since the material behaviour depends on the mode of loading (e.g. shear, tension, …) the material parameters have been derived from three different types of tests: a uniaxial tension, uniaxial compression and a shear test. These three tests cover a wide range of possible deformations. Fig. 2 shows the second over the first strain invariant for the three tests and the area of possible deformations in grey.

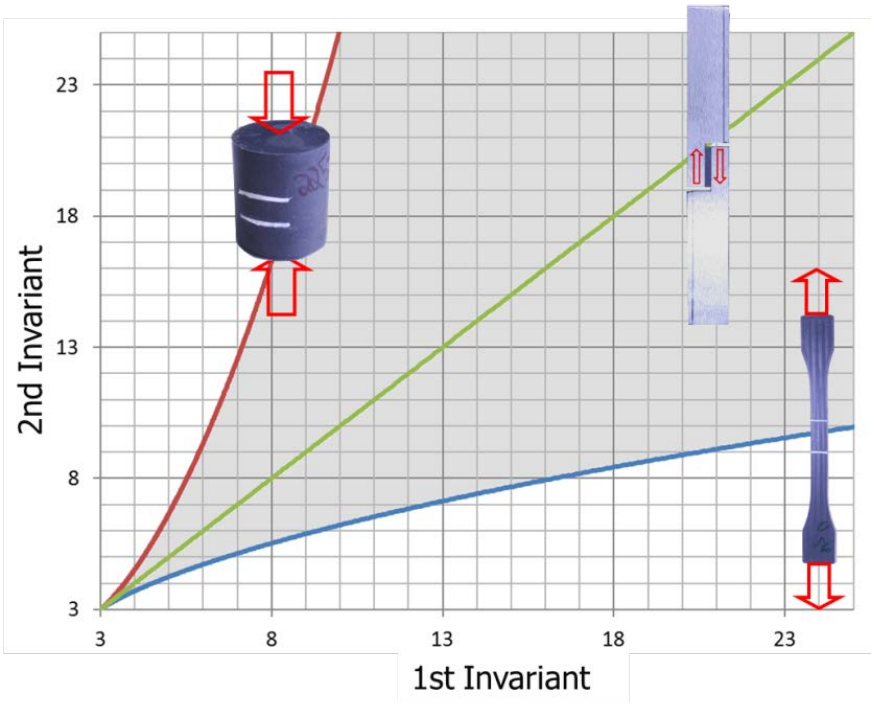

Fig. 2 2nd over 1st invariant for the three performed tests and possible deformations in grey.
see also (Treloar 1975, Vöhringer 2009, Baaser 2010, Weiß et al. 2010)

The tests have been performed at three different temperatures (-20 °C, RT, +80 °C) and material parameters have been derived for each set of tests by use of a least square minimization over both, the stress strain behaviour of all three tests and the transversal contraction behaviour in the tension tests. All measurements have been performed using contactless optical measuring devices. For Kömmerling HelioBond PVA 200 D the best results were achieved with the Ogden-Model (N = 3) (cf. (Dassault Systemes Simulia Corp. 2016)). Fig. 3 shows the stress strain behaviour of the considered material models compared with the results from the uniaxial tests.

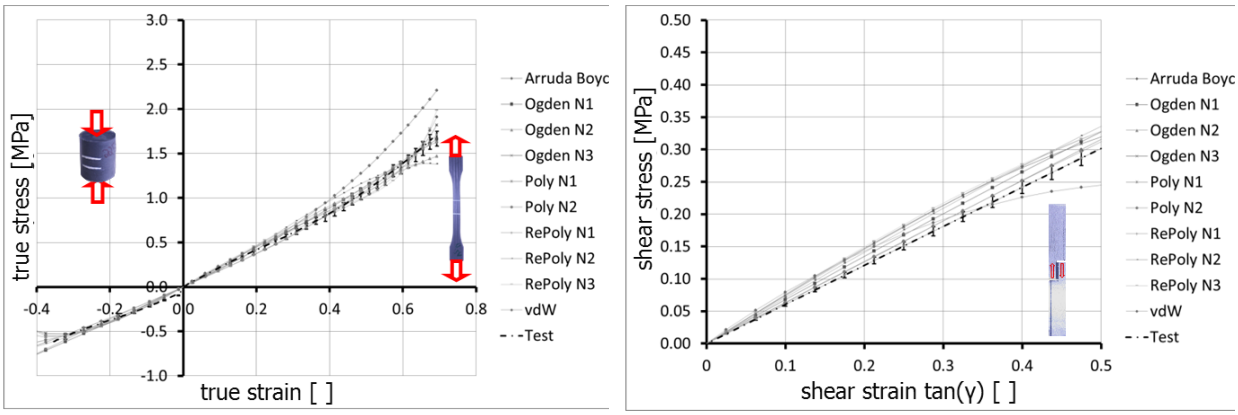

a) b)

Fig. 3 Stress-Strain behavior for the considered hyperelastic models compared with the experimental data

The load-history dependent material behaviour is covert using a Mullins-Effect Model (Arrhenius 1889, Ogden and Roxburgh 1999, Dassault Systemes Simulia Corp. 2016) which is also available in commercial FE-Software. The parameters are identified using a least square minimization, analogue to the identification of the non-history-dependent hyperelastic material behaviour described above. Although the rate dependency of the material behaviour for the given load situations is of minor influence compared to the temperature and history dependency, in this work a time temperature shift, based on the Arrhenius-Equation (Dassault Systemes Simulia Corp. 2016), was used to model this behaviour. The parameters have been derived from DMTA analysis with different temperatures and frequencies. More details about the material model used and the way the parameters have been identified can be found in (Scherer 2014).

For a proof of strength in addition to a suitable material model a proper limiting value is needed. For hyperelastic materials the use of stresses or equivalent stresses can deliver incorrect results (Scherer 2014). Therefore in this work both the principal strains and the strain energy density are used and compared. The limiting values will be calculated from the design values for Kömmerling HelioBond PVA 200 D determined according to ETAG 002 (Table 1) as below.

Table 1: Design values according to ETAG 002 for Kömmerling HelioBond PVA 200 D

Properties & Characteristics	Symbol	Value
Design stress in dynamic shear	τ_{des}	0.21 MPa
Elastic modulus in tension or compression tangential to the origin	E_0	2.8 MPa
Elastic modulus in shear tangential to the origin	G_0	0.93 MPa

Using the described material model and the determined parameter from above the design value of 0.21 MPa (engineering shear stress) corresponds to an engineering shear strain of:

$$tan(\gamma) = 0.21 \tag{4}$$

Where $\tan(\gamma)$ represents the shear strain. Furthermore the strain characteristic of a simple shear situation in terms of principal stretches can be written as shown in equations 5 to 8

$$\lambda_1 = \lambda_S \tag{5}$$

$$\lambda_2 = \frac{1}{\lambda_S} \tag{6}$$

$$\lambda_3 = 1 \tag{7}$$

$$\gamma = \lambda_S - \frac{1}{\lambda_S} \tag{8}$$

where λ_i are the principal stretches and γ is the shear angle.

Using equations 5 to 8 with the definition of the strain energy density according to Ogden (equation 9) with the determined material parameters and the design value in equation 4 gives us equation 10.

$$U_{dev}(\bar{\lambda}_1, \bar{\lambda}_2, \bar{\lambda}_3) = \sum_{i=1}^{N} \frac{2\mu_i}{\alpha_i^2}\left(\bar{\lambda}_1^{\alpha_i} + \bar{\lambda}_2^{\alpha_i} + \bar{\lambda}_3^{\alpha_i} - 3\right) \quad (9)$$

$$U_{dev} = 0.209\ \frac{J}{mm^3} \quad (10)$$

Where $\bar{\lambda}_1$ are the deviatoric principal stretches and $\mu_i$and α_i are material parameters. The strain energy density from equation 10 can now be used as a limiting value e.g. a design value for the dimensioning of an adhesive joint. Although the dimensioning according to ETAG 002 is an approach that uses average stresses per reference area, this value can give an idea on how the local load condition is compared to a load condition that can be approved in accordance with ETAG 002. As localization increases observed maximum stress and strain levels the use of global limiting values is considered to be conservative.

2.2. Global Model

In this part of the work a Finite-Elements-Model of the whole solar thermal collector module (1000 mm x 600 mm) shell be investigated and the model and the calculation results described further on.

2.2.1. Model Description

Since the geometry is symmetric and the critical dead-load is orthogonal just one quarter of the module is modelled and proper boundary conditions are assigned. The model is depicted in Fig. 4 a) (mirrored) and the quarter of the module actually used is shown in Fig. 4 b).

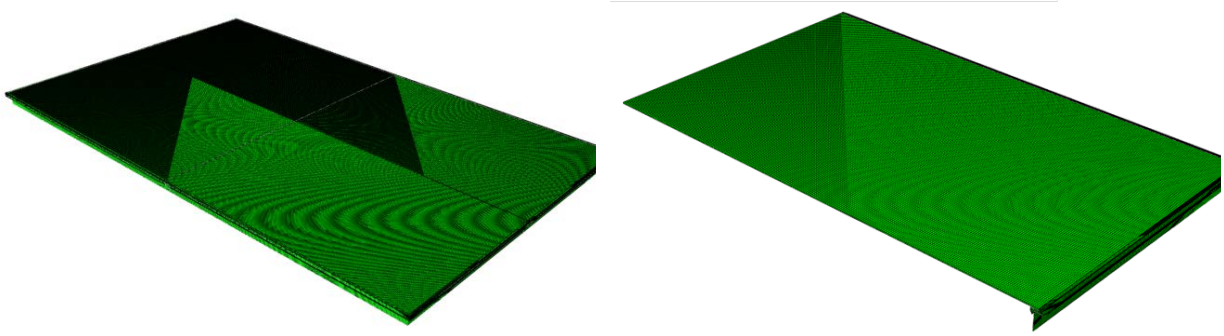

a) b)

Fig. 4 a) mirrored model for the whole module, b) FE-model (one quarter of the model)

For the discretization of the glass pane continuum shell elements are used. The frame is discretized with 3D continuum elements and the adhesive with 3D hybrid elements (ref. to (Dassault Systemes Simulia Corp. 2016)). For both, the aluminium frame and the glass a linear elastic material model is used. The material model for the adhesive is the one described in chap. 2.1. Table 2 gives an overview of the used element types and sizes and Fig. 5 shows a detail of the model with the different parts.

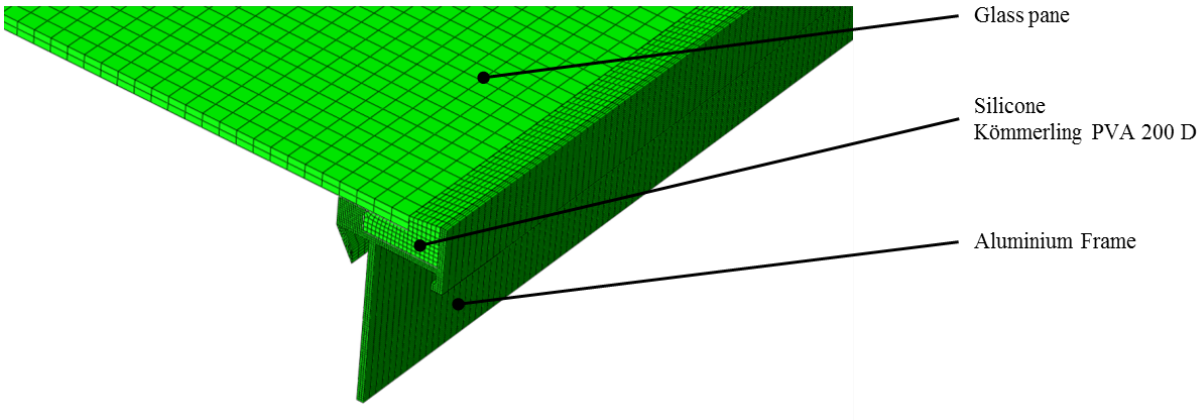

Fig. 5 Detail of the global model with indication of the different parts

Table 2: Used Element Types and Sizes for the Global Model (ref. to (Dassault Systemes Simulia Corp. 2016))

Part	Element Type	Average Element Size	Remarks
Frame	C3D8R	0.5 mm	Continuum Elements, reduced integration
Adhesive	C3D8RH	1 mm	Continuum Elements, hybrid formulation, reduced integration
Glass	SC8R	2 mm	Continuum Shell Elements

For the global model two different load cases are considered. One representing the situation of combined dead load and wind suction and the other one with combined dead-load, wind pressure and snow load. The model has been calculated at -20 °C, room temperature and +80 °C. Table 3 shows the different load cases that have been considered for the global model. To stay on the safe side even Load-Case 2 has been calculated for 80 °C although a combination of 80 °C in the adhesive joint with a snow load present on the glass pane is unlikely.

Table 3: Load 2Cases for the global model

Load Case	Direction	Surface Load	Temperatures	Remarks
1	tension	2400 Pa + dead load	-20 °C to 80 °C	dead load + wind (suction)
2	pressure	5200 Pa + dead load	-20 °C to 80 °C	dead load + wind (pressure) + snow

2.2.2. Results

For the adhesive joint dimensioning the principal (logarithmic) strains are evaluated, since the evaluations of strains has proven more suitable for identifying a critical situation than the evaluation of stresses (Scherer 2014). Fig. 6 and Fig. 7 show the results for both load cases (here with 80 °C since these are the load cases with the highest strains). The Figures show cut sections on the long (a)), the short edge (c)) and through the bisection of the corner (b)).

a)

b)

c)

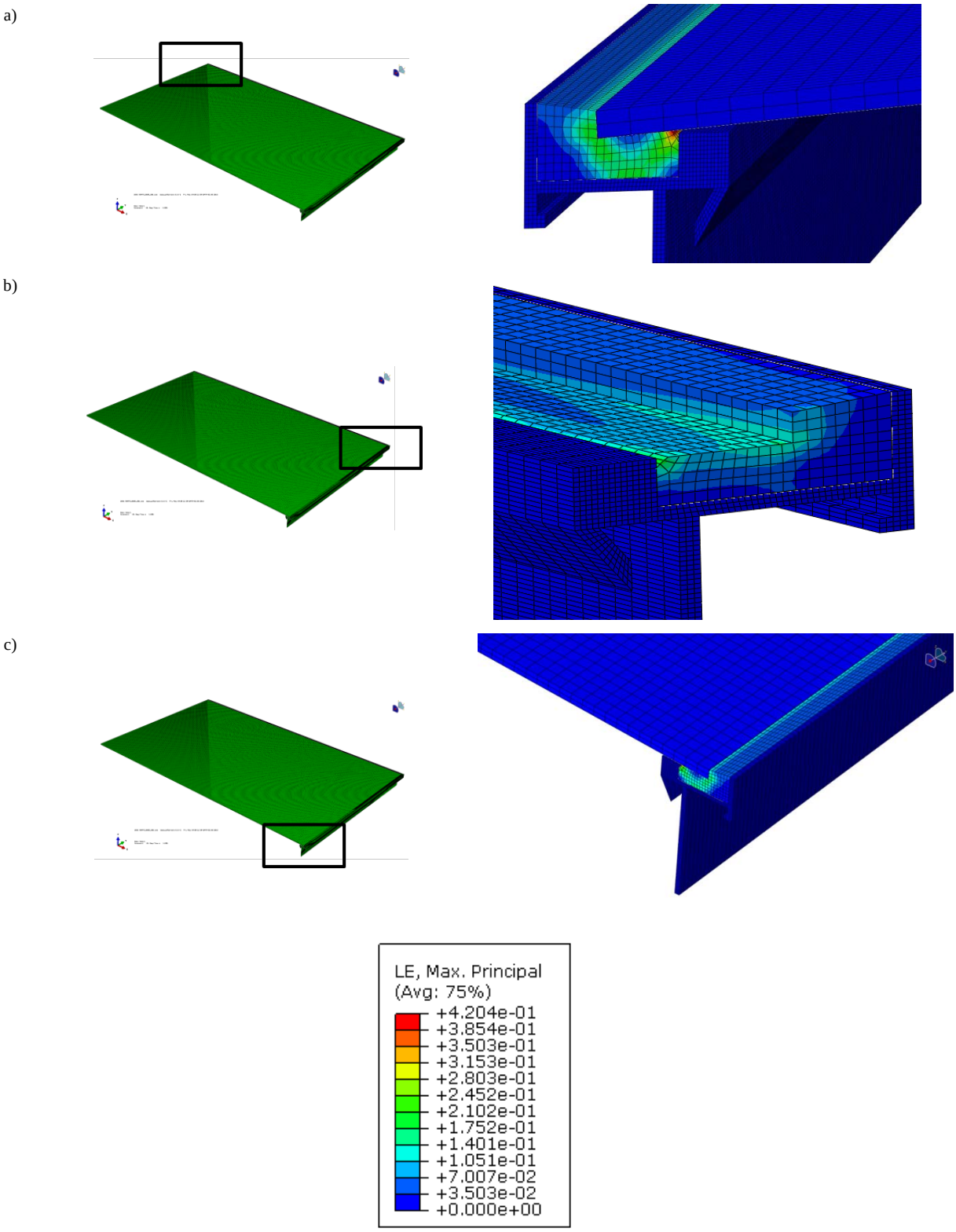

Fig. 6 a), b) and c) Results for principal strains from the FE-Analysis for the global model, Load-Case 1, (deformation scaled by factor 2); [ ]

a)

b)

c)

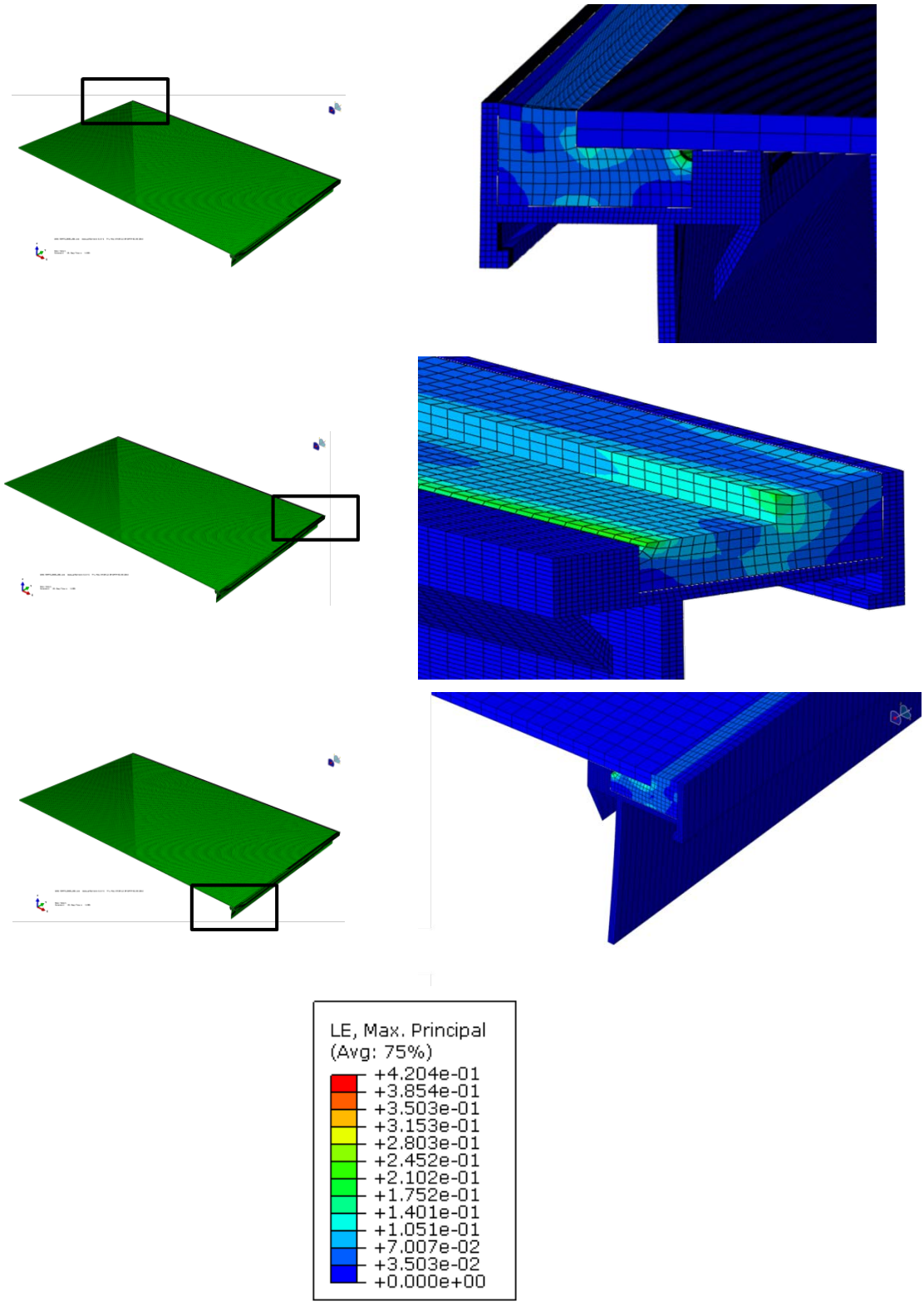

Fig. 7 a), b) and c) Results for principal strains from the FE-Analysis for the global model, Load-Case 2, (deformation scaled by factor 2); [ ]

The simulations give a maximum principal (logarithmic) strain within the adhesive joint of

$$max(\varepsilon_l) = 0.2002 \qquad (11)$$

To compare the load situation in this module with the design values according to ETAG 002 the strain energy density is calculated for the adhesive joint. Fig. 8 a) to c) show the distribution of the strain energy density.

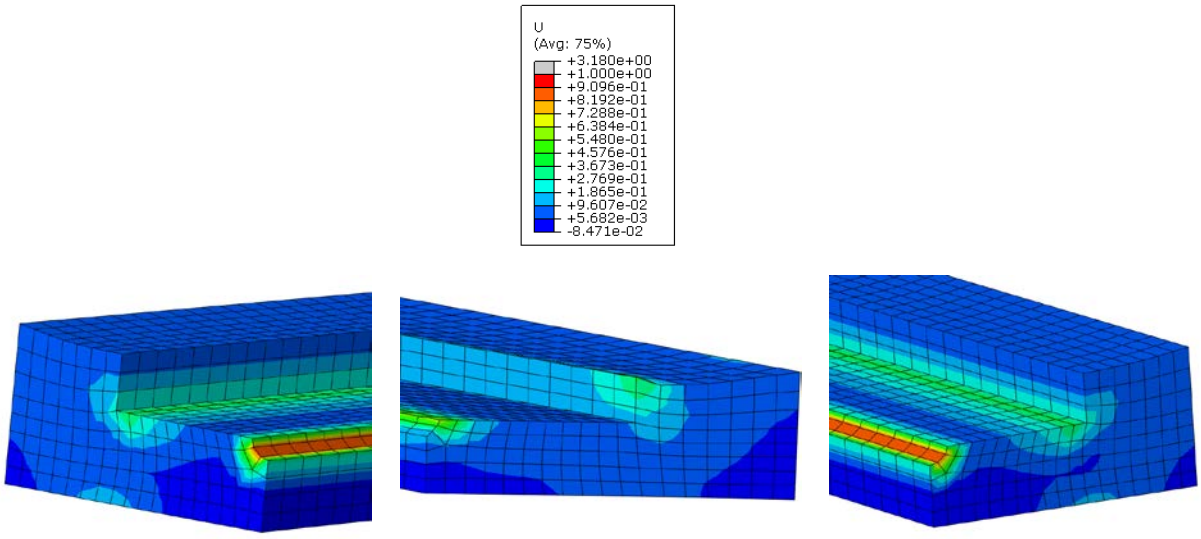

a) b) c)

Fig. 8 distribution of the strain energy density for cross-section of the long edge (a)), the bisection of the corner (b)) and the short edge (c)); Load-Case 2, 80 C; (deformation scaled by factor 2); [J/mm^3]

As we can see in the pictures above the strain energy density is lower than the calculated design value from equation 10 in predominant parts of the cross-sections. Nevertheless small shares of the cross-sections show higher values. Since the dimensioning according to ETAG 002 is based on average values related to the full reference area and the average values in the cross-sections of the strain energy density are lower than the calculated design value from chap. 2.1, in this work the considered geometry will be further investigated.

Since the restriction of lateral contraction is at its maximum in the corner area of the adhesive joint, this detail is most critical. Therefore further investigations in this work will focus on this area. As use of computational methods for analysis of this question are limited due to numerical problems and influence of imperfections within the joints of real modules, experimental validation is necessary.

3. Experimental investigation on small components

To ensure the mechanical safety of the considered module in this work experimental tests with small components are done. The test specimens reflect the geometry of the corner area present on a whole module. The aim is to perform tests at cyclic load levels representing the maximum dynamic impact with an additional safety factor and reach $2 \cdot 10^6$ load cycles.

3.1. Small Component Test Specimens and Test Assembly

Since it requires great resources (huge testing rigs and expensive test specimens) and it is inefficient in terms of costs to perform tests with whole modules, the following tests are performed on small 100 mm x 100 mm components cut from the edge of the module. The investigations in 0 have shown that this is the area where the loads become most critical. The components will be tested on pneumatic fatigue testing machines. Those machines are depicted in Fig. 9.

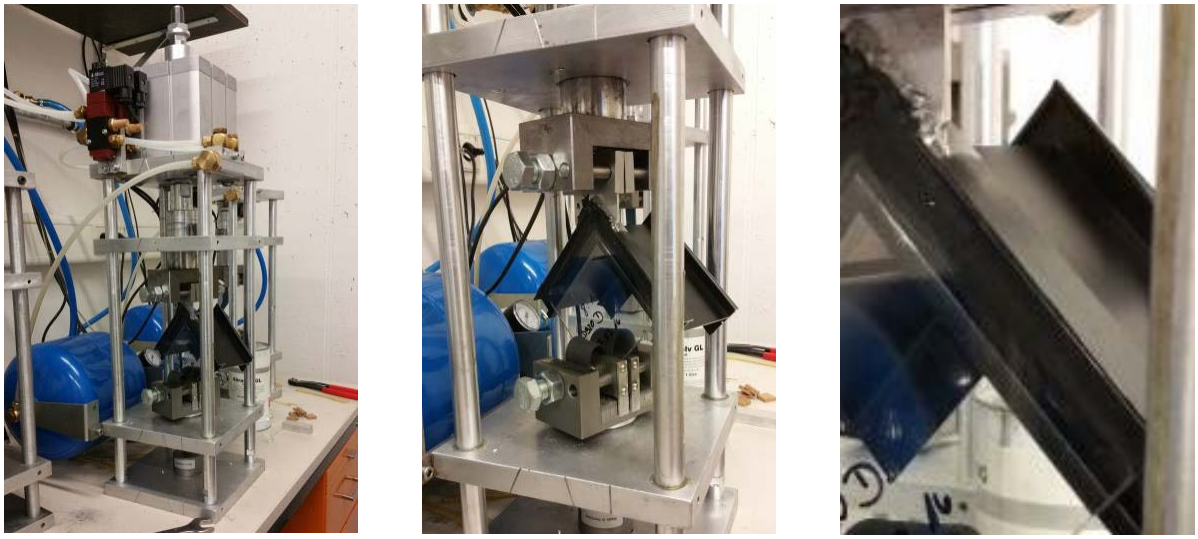

a) b) c)

Fig. 9 a), b) and c) Pneumatic testing machine with 100 mm x 100 mm test specimens

The load direction is chosen in the direction of the glass pane (in-plane), since testing in two directions is not possible with the given assembly and incurs additional expense. The chosen loads shall represent the maximum estimated loads in the modules and include a safety factor. The following chapter describes how these loads are determined. In order to ensure a worst case consideration, the tests are performed load controlled.

3.2. Determination of relevant loads and movements

The aim for the determination of the loads is to represent a worst case scenario with an additional safety factor. The calculations from the model of the whole module show that the highest principal strains in the adhesive joint occur at the middle of the long edge. At this position the adhesive joint has the lowest stiffness therefore lateral contraction is minimal at this point. The inability for the adhesive to laterally contract is at its maximum in the corner area.

In the following experiments the maximum strains from the whole model will be applied to the edge area which is the most critical position in our model. This procedure will act as the desired safety factor since this situation will not occur in the field.

Since the experiments shall be performed with force controlled parameters the required forces have to be calculated. This is done with an FE-Model of the test specimens. The model is analogue to the model described in chap. 0 the elements used are smaller and continuum elements are used for the glass pane instead of continuum shell elements. The used element types and average edge lengths are shown in Table 4.

Table 4: Used Element Types and Sizes for the Global Model (ref. to (Dassault Systemes Simulia Corp. 2016))

Part	Element Type	Average Element Size	Remarks
Frame	C3D8R	0.75 mm	Continuum Elements, reduced integration
Adhesive	C3D8RH	0.75 mm	Continuum Elements, hybrid formulation, reduced integration
Glass	C3D8R	0.75 mm	Continuum Elements, reduced integration

Fig. 11 shows the model and the resulting force-displacement curve for in-plane loading. Fig. 10 shows the logarithmic strains (a)) and equivalent stresses (b)) for an in-plane displacement of U = 0.56 mm. At this displacement shear deformations are found corresponding to the maximum deformations that were determined in the global model at the long edge.

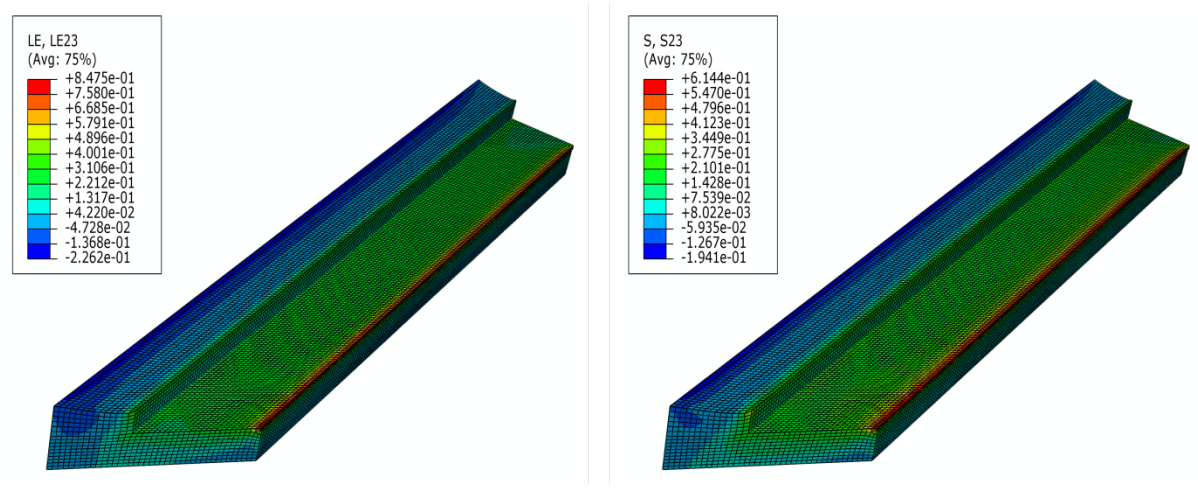

a) b)

Fig. 10 Adhesive joint logarithmic strains (a)) and stresses (b)) calculated with the model for the small components; in-plane displacement U = 0.8 mm; Stress in [MPa]

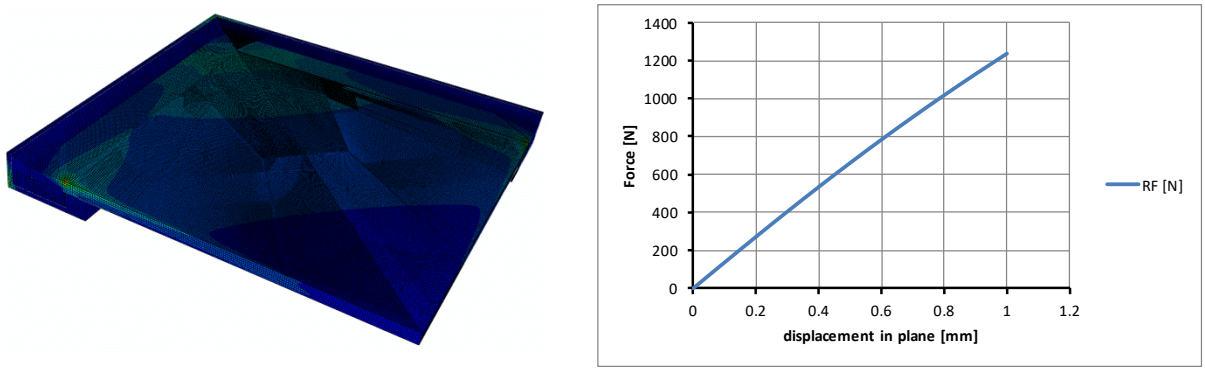

a) b)

Fig. 11 Detail of the global model with indication of the different parts

The force displacement curve in Fig. 11 b) provides the desired force for the fatigue experiments (ca. 1008 N). During the experiment the desired displacements and therefore the resulting strains will be checked by examination of the movement of the pneumatic piston.

3.3. Results of the fatigue tests

With the described test specimen and load conditions two kinds of tests are performed. One test was done with the load level that was calculated in chap. 3.2 and one with the load doubled. The results are shown in Table 5.

Table 5: Results of the fatigue tests with 100 mm x 100 mm component test specimen

Load	Multiple of Desired Load (chap. 3.2)	Cycle Frequency	No of Load Cycles	Results
1008 N	1	1 Hz	$2.0 \cdot 10^6$	No failure, no visible crack
2016 N	2	1 Hz	$2.0 \cdot 10^6$	No failure, no visible crack
2016 N	2	1 Hz	$3.0 \cdot 10^6$	No failure, visible crack
2016 N	2	1 Hz	$5.1 \cdot 10^6$	Failure

The results from Table 5 show that the required load cycles with the load level from chap. 3.2 has been reached. Even an experiment with twice the load does not show failure or visible cracks. Only after $3 \cdot 10^6$ with twice the calculated load visible cracks can be observed. A total failure occurs after $5 \cdot 10^6$ cycles with the double load.

4. Conclusion

The aim of this work is the approval of an adhesive joint used to join a glass pane in a solar thermal module to an aluminium frame. The joint geometry is L-shaped and therefore out of the scope of ETAG 002 which makes it necessary to come up with an approach that is valid for more complex geometries. In this work a hyperelastic material model is used to describe the material behaviour of the adhesive Kömmerling HelioBond PVA 200 D and a strain energy density based approach makes it possible to compare the load level in a complex geometry with the allowable load level according to ETAG 002. In the following this material model is used in numerical simulations describing the whole frame, glass pane and adhesive joint of the solar thermal module in order to investigate the load distribution within the L-shaped adhesive joint. By comparing the deformations in this global model with the deformation of small section cuts from the corner area of the module using a more detailed finite element model made it possible to perform experiments with small section cuts. This method is much more cost effective than testing a whole module and the results can be transferred to other designs. The fatigue tests with small component joints with Kömmerling HelioBond PVA 200 D show that the adhesive joint is capable of withstanding the required loads. Even doubling the load did not cause visible damage after the desired number of load cycles.

The shown systematic approach gives an opportunity to dimension elastic adhesive joints with geometries that are not allowed according to EOTA ETAG 002 and therefore opens the door for more complex and sophisticated designs.

References

Arrhenius, S.: Über die Reaktionsgeschwindigkeit bei der Inversion von Rohrzucker durch Säuren Zeitschrift für Physikalische Chemie **4**, 226–248 (1889)

Arruda, E.M., Boyce, M.C.: A three-dimensional constitutive model for the large stretch behavior of rubber elastic materials Journal of the Mechanics and Physics of Solids **41**(2), 389–412 (1993). doi: 10.1016/0022-5096(93)90013-6

Baaser, H.: Simulationsmodelle für Elastomere ATZ - Automobiltechnische Zeitschrift(Ausgabe 05/2010), 364–369 (2010)

Dassault Systemes Simulia Corp.: Abaqus Analysis User Manual (2016)

EOTA - European Organisation for Technical Approvals: ETAG 002 - Guideline for European Technical Approval for Structural Sealant Glazing Kits (SSGK), Brussels (2012)

Hagl, A.: Understanding complex adhesive behaviour: Case study U-type bonding geometry Challenging Glass, 227–240 (2008)

Klosowski, J.M., Wolf, A.T.: Sealants in construction. Civil engineering. CRC Press, Boca Raton, FL (2016)

Mullins, L.: Effect of stretching on the properties of rubber Rubber Chemistry and Technology **21**(2), 281–300 (1948)

Ogden, R.W., Roxburgh, D.G.: A pseudo-elastic model for the Mullins effect in filled rubber Proceedings of the Royal Society of London **1999**(1988), 2861–2878 (1999)

Ogden, R.W.: Large Deformation Isotropic Elasticity - On the Correlation of Theory and Experiment for Incompressible Rubberlike Solids Proceedings of the Royal Society A: Mathematical, Physical and Engineering Sciences **326**(1567), 565–584 (1972). doi: 10.1098/rspa.1972.0026

Scherer, T.: Werkstoffspezifisches Spannungs-Dehnungs-Verhalten und Grenzen der Beanspruchbarkeit elastischer Klebungen, Technische Universität Kaiserslautern (2014)

Treloar, L.R.G.: The physics of rubber elasticity, 3rd edn. Monographs on the physics and chemistry of materials. Clarendon Press, Oxford (1975)

Vöhringer, M.-C.: Prüfung und Beschreibung des mehrachsigen mechanischen Verhaltens von Elastomeren für die Finite-Elemente-Methode. Dissertation, 1st edn. IKV-Berichte aus der Kunststoffverarbeitung, vol. 199. Verl.-Gruppe Mainz, Aachen (2009)

Weiß, R., Osen, E., Baaser, H.: FEM–Simulation von Elastomerbauteilen ATZ - Automobiltechnische Zeitschrift(Volume 103, Issue 3,), 242–247 (2010)